ISSN 1087-6596, Glass Physics and Chemistry, 2007, Vol. 33, No. 1, pp. 86–95. © Pleiades Publishing, Ltd., 2007.
Original Russian Text © A.E. Galashev, V.A. Polukhin, I.A. Izmodenov, O.R. Rakhmanova, 2007, published in Fizika i Khimiya Stekla.

Molecular Dynamics Simulation of the Physicochemical Properties of Silicon Nanoparticles Containing 73 Atoms

A. E. Galashev[a], V. A. Polukhin[b], I. A. Izmodenov[c], and O. R. Rakhmanova[c]

[a] *Institute of Thermal Physics, Ural Division, Russian Academy of Sciences,*
ul. Amundsena 106, GSP-828, Yekaterinburg, 620219 Russia
e-mail: galashev@ecko.uran.ru
[b] *Institute of Metallurgy, Ural Division, Russian Academy of Sciences,*
ul. Amundsena 101, GSP-828, Yekaterinburg, 620219 Russia
[c] *Institute of Industrial Ecology, Ural Division, Russian Academy of Sciences,*
ul. S. Kovalevskoi 20a, GSP-594, Yekaterinburg, 620219 Russia

Received July 1, 2005

Abstract—The physicochemical properties of 73-atom silicon nanoparticles that have a crystal structure, a random atomic packing, and a packing formed by inserting a 13-atom icosahedron into a 60-atom fullerene are investigated using the molecular dynamics method. Analysis of the behavior of the internal energy, the radial distribution function, the distribution of bond angles, and the specific heat at a constant pressure C_p in the temperature range 10–1710 K indicates that a crystalline nanoparticle undergoes melting at a temperature of 710 K and that the structural transformations occurring in particles with an irregular atomic packing exhibit specific features. It is demonstrated that the temperature dependence of the self-diffusion coefficient follows a linear behavior. Local deviations from the linear behavior are most pronounced for the crystalline nanoparticle.

DOI: 10.1134/S1087659607010130

INTRODUCTION

The particular interest expressed by researchers in silicon nanoparticles is associated primarily with the use of these objects in optoelectronics. Owing to the small sizes of these particles, their physicochemical properties are substantially affected by the quantum effects that arise on scales of characteristic physical lengths, such as the mean free path of electrons and phonons, the wavelength of optical radiation, etc. Carbon, silicon, and germanium belong to the same group of the periodic table and their crystals have identical diamond-like structures. However, the properties of these macrocrystals differ substantially. Moreover, the behaviors of nanocrystals also differ radically. Carbon forms fullerenes and nanotubes, whereas these structures are unstable in the case of silicon and germanium [1]. Computer simulations predict that silicon and germanium fullerenes have a considerably lower stability. According to Chen et al. [2], Si_{60} and Ge_{60} fullerenes undergo decomposition at temperatures of 700 and 200 K, respectively. Nishio et al. [3] and Park et al. [4] demonstrated that nanocrystals or amorphous nanoaggregates, i.e., quantum dots, closely packed in the silicon nitride and silicon dioxide are able to amplify incident light. The quantum dots take their name because their properties are similar to the properties of individual atoms in many respects. These structures can be treated as three-dimensional quantum wells. They are responsible for the energy quantization even at distances that are several hundred times larger than the lattice constant of the material. The quantum dot can be considered an electron trap. Each individual electron trapped by the quantum dot does not possess the energy required to leave this dot. The smaller the quantum dot, the higher the potential energy necessary for the electron to escape from the potential well. As a rule, the diameters of the quantum dots prepared from the semiconductor materials used at present vary from 1 to 10 nm; i.e., the quantum dots contain from approximately 300 to 10^5–10^6 atoms.

The optical properties and the electronic structure of quantum objects (dots) depend substantially on their sizes and the arrangement of atoms in a nanoparticle. For example, the location of a luminescence peak can be controlled by varying the nanoparticle size [5]. It should be noted that the luminescence intensity for amorphous quantum dots appears to be higher than the luminescence intensity for crystalline quantum dots. Materials with the properties controlled by the sizes of quantum dots contained in them, as well as by the arrangement of atoms in these objects and the symmetry of nanoparticles, can be used in luminescent devices, lasers, diodes, sensors, and switches. Moreover, they can be used for writing and reading of optical information.

Parameters of the Tersoff potential for silicon

A, eV	B, eV	λ_1, nm^{-1}	λ_2, nm^{-1}	λ_3, nm^{-1}	n	c	d	R, nm	D, nm	β	σ, nm	ε, eV
3264.7	95.373	32.384	13.258	13.258	22.956	4.8381	2.0417	0.3	0.02	0.33675	0.37	0.01182

In this work, we investigated the temperature dependences of the physicochemical properties of silicon nanoparticles in the form of a fragment of a diamond-like lattice, a particle with a random atomic packing, and a compact nanoassembly with clearly pronounced threefold, fivefold, and sixfold symmetries. In the case of free boundaries, silicon nanoparticles with the last-mentioned structures can be unstable. However, when they form a dense extended structure, it is possible to prepare a slowly relaxing irregular material, i.e., a glass.

The purpose of the present work was to investigate the structural and kinetic properties of silicon nanoparticles that contain 73 atoms and represent fragments of a diamond-like lattice or a random atomic packing, as well as a nanoassembly formed by inserting a 13-atom icosahedron into a 60-atom fullerene.

THE MOLECULAR DYNAMICS MODEL

In essence, molecular dynamics calculations are computer calculations that make it possible to solve numerically the many-body problem in mechanics. In the model, the positions and velocities of atoms are represented as time functions. The microscopic behavior of a system is calculated by solving the differential equations of motion with the use of initial positions and velocities of atoms and interatomic interaction forces. The molecular dynamics calculations are characterized as a determinate process (accurate to within the computational error), because no stochastic factors are included in the atomic motion. Integration of the equations of motion was performed using the fourth-order Runge–Kutta method. The time step Δt was equal to 10^{-16} s.

Tersoff [6, 7] proposed a new form of the interatomic pair potential with due regard for many-atom correlations. The main idea is that, in real systems, the strength of each bond depends on the local environment, so that bonds formed by an atom with many neighbors are weaker than those formed with several nearest neighbors. As follows from computer simulations, the properties of silicon that would be consistent with experimental data are difficult to reproduce by using a unified empirical potential describing the crystalline, amorphous, and liquid phases [8]. The use of the Tersoff potential for nanoparticles without cavities can lead to incorrect results. In this respect, the potential energy of the system was described by a combination of the Tersoff potential V_{ij} and the Lennard-Jones potential V_{ij}^{LJ}; that is,

$$U = \frac{1}{2}\sum_{i \neq j}(V_{ij} + kV_{ij}^{\mathrm{LJ}}), \qquad V_{ij} = f_C(r_{ij})\lfloor f_R(r_{ij}) + b_{ij}f_A(r_{ij})\rfloor, \tag{1}$$

where $k = 1$ for the nanoassembly composed of a 60-atom fullerene and a 13-atom icosahedron at interatomic distances $r_{ij} < (R - D) = 0.28$ nm; $k = 0$ in all other cases, including the two other systems; r_{ij} is the distance between the ith and jth atoms; f_A and f_R are the attractive and repulsive pair potentials, respectively; and f_C is the smooth cut-off function. The potentials f_A and f_R in an explicit form are represented by the Morse potentials

$$f_R(r) = Ae^{-\lambda_1 r}, \quad f_A(r) = -Be^{-\lambda_2 r}, \tag{2}$$

$$f_C(r) = \begin{cases} 1, & r < R - D \\ \frac{1}{2} - \frac{1}{2}\sin\left[\frac{\pi}{2}(r - R)/D\right], & R - D < r < R + D \\ 0, & r > R + D. \end{cases} \tag{3}$$

The parameters A and B determine the repulsive and attractive forces, respectively. The parameters R and D are chosen in such a way as to include only the layer of the first nearest neighbors in the bulk structures of silicon, graphite, and diamond. The smooth cut-off function f_C decreases from 1 to 0 in the range $R - D < r < R + D$. The main feature of this potential is the presence of the term b_{ij}. The bonding force depends on the local environment and decreases when the number of neighbors is large. This behavior of the bonding is governed by the term b_{ij}, which increases or decreases the ratio between the attractive and repulsive forces according to the relationship

$$b_{ij} = \frac{1}{(1 + \beta^n \varsigma_{ij}^n)^{1/2n}}, \tag{4}$$

where

$$\varsigma_{ij} = \sum_{k \neq i, j} f_C(r_{ij})g(\theta_{ijk})e^{[\lambda_3^3(r_{ij} - r_{ik})^3]}, \qquad g(\theta) = 1 + \frac{c^2}{d^2} - \frac{c^2}{[d^2 + (\cos\theta)^2]}. \tag{5}$$

The term ς_{ij} characterizes the effective coordination number of the ith atom, i.e., the number of the nearest neighbors. This number is determined with allowance made for the relative distance between two neighbors $r_{ij} - r_{ik}$ and the bond angle θ. The function $g(\theta)$ describes the dependence of the coordination number on the bond angle. The parameter d characterizes the rate of change of the function $g(\theta)$. The parameter c specifies the dependence of the force on the angle θ. The parameters of the potential V_{ij} were chosen by fitting the theoretical and experimental data obtained for real and hypothetical configurations. These data involved the bonding energy, the lattice constant, and the bulk modulus. The parameters of the Tersoff potential used for silicon are presented in Table 1 [7]. Moreover, this table also involves the parameters σ and ε of the Lennard-Jones potential for silicon [9]. It should be emphasized that the Lennard-Jones interaction (repulsion) was taken into account only in the case where the atoms approach each other to a distance $r < (R - D)$ when simulating the nanoassembly consisting of the icosahedron and the fullerene. The reason is that the Tersoff potential is applicable for simulating systems in which, on average, there are three or four covalent bonds for every atom [10]. In the initial packing composed of the fullerene with the inscribed extended icosahedron, there are five fullerene atoms located at the distance equal to the bond length $L_b = 0.24$ nm for each atom positioned on the icosaherdron surface. For an atom of the icosahedron surface, the five nearest neighbors also lying on the icosahedron surface can be disregarded, because the distance to these atoms is ~1.9 times larger than the bond length L_b and the distance from the icosahedron center to atoms on its surface is 1.8 times larger than the bond length L_b. The attraction of the fullerene by the icosahedron is provided by 60 bonds. In the absence of the Lennard-Jones repulsion at small distances, the molecular dynamics calculations lead to an inadequate behavior of the nanoassembly. In this case, atoms even at sufficiently low temperatures rapidly approached each other to impermissibly small distances. As a consequence, the internal pressure increased rapidly and the potential energy reached high positive values. A fast disturbance of the local environment of atoms located on the icosahedron surface is associated not only with their quintuple bonds with the fullerene but also with the fact that the angle between the bonds differs from the tetrahedral angle (109.47°). As a result, the nanoassembly underwent collapse in the course of the molecular dynamics calculations when using only the Tersoff potential with the parameters for silicon. However, the use of the Tersoff potential with the parameters for carbon in the molecular dynamics calculations does not result in the collapse of the corresponding configuration. The situation can be corrected, to some extent, by including the Lennard-Jones contribution responsible for the additional repulsion at distances smaller than $R - D$.

Three series of calculations were performed for silicon nanoparticles. The temperature of the initial state for each series of calculations was taken equal to 10 K. The duration of the calculations at each temperature was equal to 1000000 time steps or 100 ps. The final atomic configuration obtained at a lower temperature served as the initial configuration for the subsequent calculations at a higher temperature. In the calculations, the temperature was increased in steps of 100 K. The last calculations were carried out at a temperature of 1710 K. In the first series of calculations, a fragment composed of a particular site with 72 nearest neighbors in the diamond lattice was used as the initial configuration. In the initial state, the density of the crystalline nanoparticle corresponded to that of the macrocrystalline material. In the second series of calculations, a fragment with a random atomic packing served as the initial configuration. This configuration of the nanoparticle was produced by filling a spherical region of the corresponding radius with silicon atoms by using a random-number generator. In the initial state, the minimum distance between silicon atoms in the random packing did not exceed the minimum distance in the corresponding macrocrystal (0.24 nm). As a result (and also in view of a decrease in the time of filling the sphere), the initial nanoparticle had a looser atomic packing. The nanoparticle density was no higher than 0.6 of the density of the silicon nanocrystal. In the third series of calculations, the initial configuration of the nanoparticle was represented by the nanoassembly composed of a 60-atom fullerene into which a 13-atom icosahedron was inserted. The minimum distance between the atoms in this nanoassembly corresponded to the minimum distances between atoms in the silicon macrocrystal.

THE ENERGY, THE VOLUME, AND THE SPECIFIC HEAT AT A CONSTANT PRESSURE C_P

The temperature dependences of the potential energy U and the volume V for the silicon nanoparticles under investigation are plotted in Figs. 1a and 1b, respectively. The energies for the nanoparticle with the random atomic packing and the nanoassembled nanoparticle are negative in sign over the entire range of temperatures. The dependence $U(T)$ for the nanoparticle with the initial crystal packing exhibits a sharp peak with $U > 0$ at the temperature $T = 710$ K. In the temperature range corresponding to this peak 500 K $\le T \le$ 900 K, the potential energy U for the crystalline nanoparticle is higher than those for the other nanoparticles. Similarly, the potential energy for the nanoparticle with the random atomic packing in the temperature range of the main peak 1100 K $\le T \le$ 1300 K in the dependence $U(T)$ is higher than the potential energies for the other nanoparticles in this temperature range. In all the other cases, the potential energy of the nanoassembled nanoparticle is higher than those for the other nanoparticles.

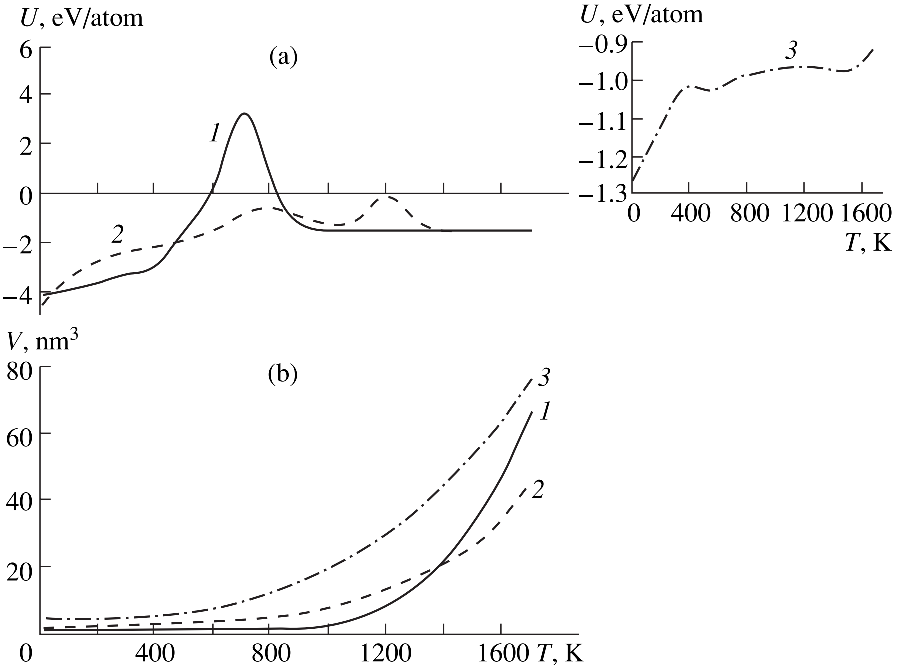

Fig. 1. Temperature dependences of (a) the potential energy of silicon nanoparticles and (b) the volume containing 73-atom nanoparticles: (*1*) particle with a diamond-like structure, (*2*) particle with a random atomic packing, and (*3*) nanoassembly composed of a 60-atom fullerene and a 13-atom icosahedron.

The volume of 73-atom nanoparticles was determined as the volume of the sphere circumscribed about the center of mass of all atoms initially forming the nanoparticle. The radius of the sphere is equal to the distance from the center of mass to the center of the most distant atom. The volume of the crystalline nanoparticle increases drastically beginning with a temperature of 1010 K. This indicates that atoms evaporate from the particle. The volume of the other nanoparticles increases more smoothly with an increase in the temperature. The volume begins to increase rapidly at a temperature of 510 K for the nanoparticle formed by the fullerene and the icosahedron and at the temperature $T = 910$ K for the nanoparticle with the random atomic packing. Therefore, the crystalline nanoparticle turns out to be most stable to evaporation.

The specific heat at a constant pressure $C_p = (\partial H/\partial T)_p$ was calculated by numerical differentiation of the enthalpy $H = E + PV$ (where E is the internal energy). For a crystalline nanoparticle, the specific heat at a constant pressure C_p diverges in the vicinity of the temperature $T = 710$ K (Fig. 2a). The horizontal line in this figure indicates the experimental value of the specific heat C_p for crystalline silicon according to the data taken from [11]. The temperature dependence of the specific heat at a constant pressure C_p for a nanoparticle with the random atomic packing exhibits two maxima at temperatures of 610 and 1210 K, whose locations are indicated by the arrows in Fig. 2b. The specific heat at a constant pressure C_p for a nanoassembled particle is relatively low, especially in the temperature range $1000\text{ K} \le T \le 1300$ K (Fig. 2c).

RADIAL DISTRIBUTION FUNCTIONS

In order to provide the required spherical symmetry, the radial distribution function $g(r)$ was constructed for one atom located most closely to the center of mass of the nanoparticle. The radial distribution functions $g(r)$ obtained at a temperature of 1710 K for all three nanoparticles under investigation are depicted in Fig. 3. The insets to Fig. 3 show the radial distribution functions for these nanoparticles at an initial temperature of 10 K. The calculated radial distribution functions and the experimental radial distribution function for amorphous silicon [12] are compared in the insets to Fig. 3. The limiting distance (2.5 nm) of the range over which the radial distribution functions $g(r)$ are determined corresponds to a volume of approximately 65 nm^3 (see Fig. 1), so that the radial distribution functions reflect the contributions not only from the atoms belonging to the nanoparticles but also from the majority of evaporated atoms. As the temperature increases, the radial distribution function of the nanoparticle with the crystal packing of atoms is smeared. However, a number of peaks even at a temperature of 1710 K remain completely resolved. The distances at which the radial distribution functions $g(r)$ remain significant increase with an increase in the temperature T. This means that an increase in the temperature leads to the nanocrystal expansion attended by evaporation of atoms. The nano-

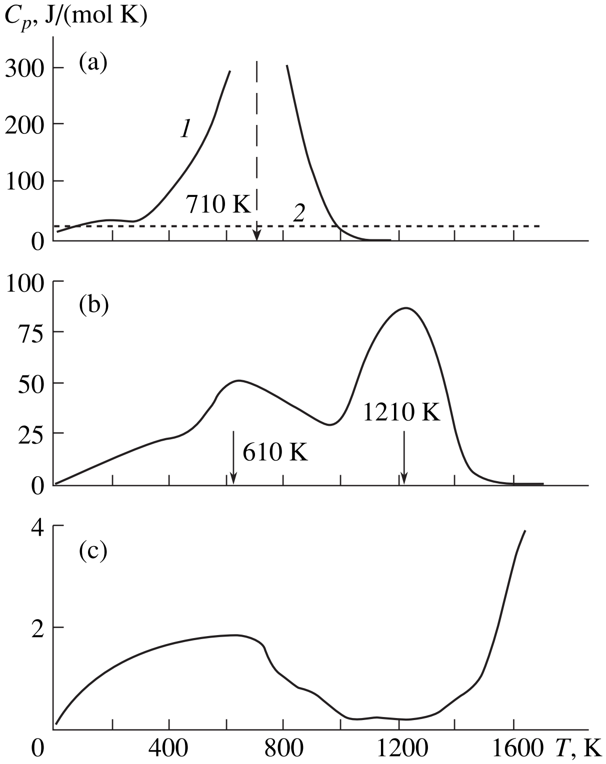

Fig. 2. Temperature dependences of the specific heat at a constant pressure $C_p(T)$ for 73-atom silicon nanoparticles in the initial state with a structure in the form of (a) a diamond-like lattice, (b) a random atomic packing, and (c) a fullerene and an inserted icosahedron according to (*1*) the molecular dynamics calculation and (*2*) the experimental data taken from [11] for crystalline silicon. Arrows indicate the location of the maxima in the dependence $C_p(T)$.

particle with the random atomic packing also becomes looser as the temperature increases. The position of the main maximum of the radial distribution function is shifted from $r = 0.25$ nm to $r = 0.28$ nm. At the initial temperature $T = 10$ K, the first peak of the radial distribution function is highest for the nanoassembled nanoparticle. This peak is shifted by 0.06 nm toward larger values as compared to the corresponding peak of the experimental radial distribution function. The shift of the first peak of the radial distribution function toward the right is equal to 0.04 nm for the nanoparticle with the random atomic packing and only 0.01 nm for the crystalline nanoparticle. The large extension of the radial distribution function for the nanoassembled particle at a temperature of 10 K is associated with the considerable displacements of the central and outer atoms due to the strong repulsion from the nearest neighbors. The number of evaporated atoms at a temperature of 1710 K is equal to eight for the nanoassembled particle, six for the nanoparticle with the random atomic packing, and four for the crystalline nanoparticle. The initial configuration of the nanoassembled particle is shown in Fig. 4a, and the configuration of this nanoparticle without evaporated atoms at the temperature $T = 1710$ K is depicted in Fig. 4b. It can be seen from these figures that an increase in the temperature is accompanied by a substantial change in the nanoparticle structure. At a high temperature, the nanoparticle has an amorphous structure in which close-packed fragments alternate with holes.

SILICON–SILICON BOND ANGLES

The bond angles φ were determined only in the case where the length of the Si–Si bonds did not exceed 0.3 nm. This bond length exceeds the distance between the nearest neighbors in crystalline silicon by approximately 27% and is close to the parameter of the Morse potential (0.30451 nm) used to describe the Si–Si interactions [13]. The mean number of bonds $\bar{n}_b$ per atom in the inner region of the nanoparticle was determined by directly counting the number of interatomic distances no larger than 0.3 nm for twelve atoms most closely located to the central atom of the nanoparticle. The mean number $\bar{n}_b$ thus determined was largest for the Si_{73} crystalline nanoparticle ($\bar{n}_b = 4.19$) at a temperature of 10 K and smallest for the nanoassembled particle ($\bar{n}_b = 1.78$) at a temperature of 1710 K. In the crystalline nanoparticle at a temperature of 10 K (see the inset to Fig. 5a), all the bond angles coincide accurate to within 1.5° with the tetrahedral angle. However, an increase in the temperature leads to a considerable change in the distribution of the bond angles φ in the nanocrystal. At $T = 1710$ K, the most intense portion of the distribution of the bond angles φ is observed in the angle range $90° \le \varphi \le 146°$ and the main peak is located at an angle of 117° (Fig. 5a). It should be noted that the maximum in the distribution of the Si–Si bond angles for the inner region (composed of 60 atoms) in the 480-atom silicon nanoparticle at a temperature of 1560 K (determined as the melting temperature) is located at an angle of 104° (Fig. 5b). This distribution was obtained by molecular dynamics calculations with the use of the Stillinger–Weber potential [14]. The distribution of the bond angles φ for the nanoparticle with the random atomic packing varies only slightly with an increase in the temperature (Fig. 5b). This suggests that the formation of a tetrahedrally ordered structure is hindered. At $T = 1710$ K, the position of the main peak remains unchanged as compared to its position at a temperature of 10 K ($\varphi = 92°$) and the intensity of this maximum decreases by 38%. The peak second in intensity in the distribution of the bond angles φ is observed at 104°. The position of this peak coincides with that of the main peak in the corresponding distribution at the melting temperature of the silicon nanoparticle [14]. As the temperature increases, the distribution of the bond angles φ broadens toward the small-angle range. Almost identical evolution of the distribution of the bond angles φ with an increase in the temperature is observed for the nanoassembled nanoparticle (Fig. 5c).

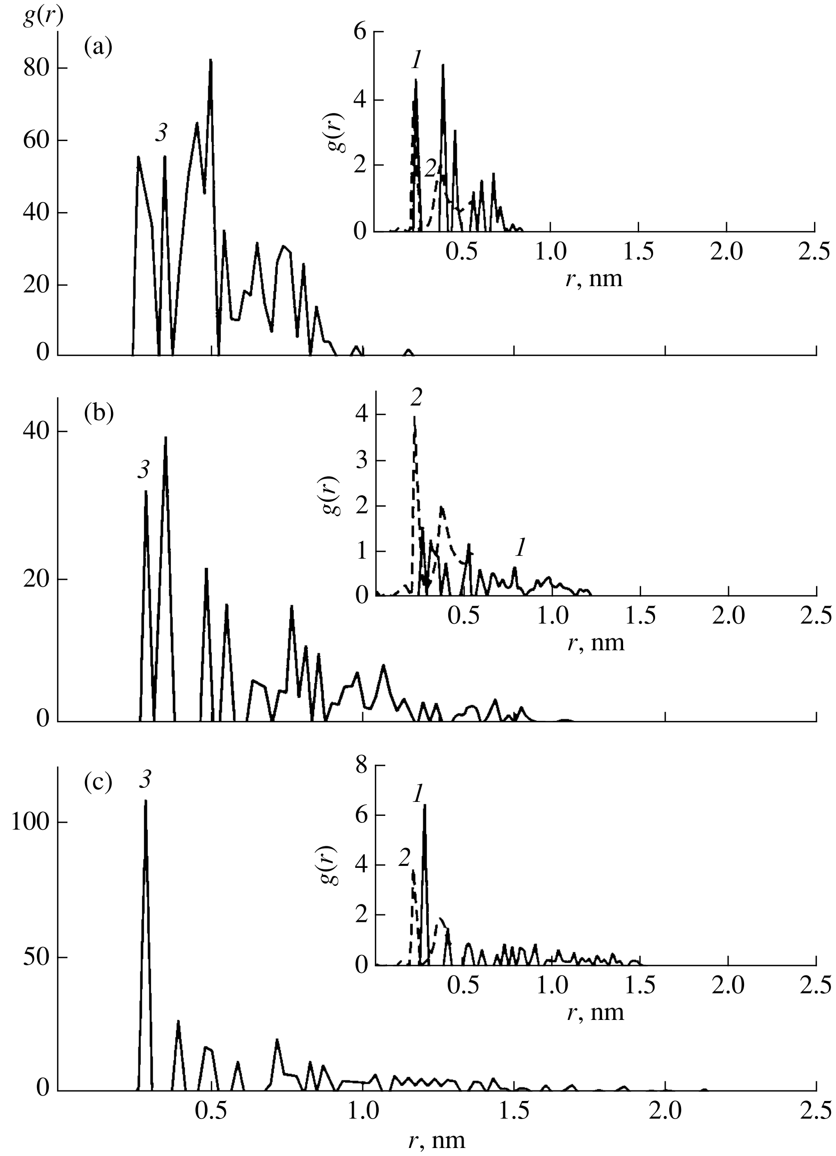

Fig. 3. Radial distribution functions $g(r)$ for 73-atom silicon nanoparticles: (a) particle with a diamond-like structure, (b) particle with a random atomic packing, and (c) nanoassembly composed of a 60-atom fullerene and a 13-atom icosahedron according to (*1*, *3*) the molecular dynamics calculations at temperatures of (*1*) 10 and (*3*) 1710 K and (*2*) the experimental data taken from [8] for amorphous silicon.

In this case, as the temperature increases from 10 to 1710 K, the intensity of the sharp peak located at an angle of 92° decreases by 29% and the distribution of the bond angles φ broadens toward the small-angle range up to 36°. The peak second in intensity in the distribution of the bond angles φ at a temperature of 1710 K is observed at an angle of 113°.

THE SELF-DIFFUSION COEFFICIENT

The self-diffusion coefficients of atoms were determined from the relationship

$$D = \lim_{t \to \infty} \frac{\langle \Delta r^2 \rangle}{6t}, \qquad (6)$$

where $\langle \Delta r^2 \rangle$ is the mean-square atomic displacement and $t = 50$ ps is the time interval in which the displacement occurs. The atomic mobility in the nanoparticles under investigation increases almost linearly with an increase in the temperature (Fig. 6). In the case of the regular atomic packing, local deviations of the temperature dependence of the self-diffusion coefficient of atoms $D(T)$ from the linear behavior are more pronounced. For each 73-atom nanoparticle, the self-diffusion coefficient D is more than two times larger than the experimental self-diffusion coefficient of atoms on the surface of crystalline silicon at a temperature of 1273 K [15].

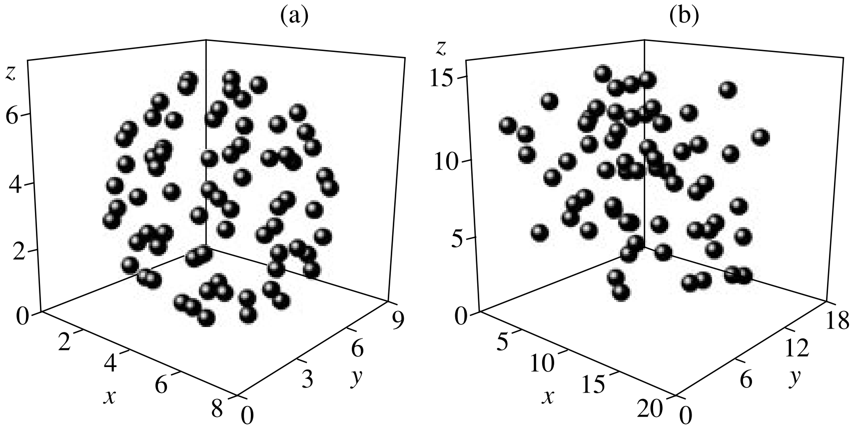

Fig. 4. Configurations of the nanoassembled silicon nanoparticle at temperatures of (a) 10 (instant of time, 1 ps) and (b) 1710 K (instant of time, 100 ps). The atomic coordinates are given in angströms.

DISCUSSION OF THE RESULTS

The difference in the initial structure of the nanoparticles is responsible, to a considerable extent, for the difference in their physicochemical properties. The intense peak in the temperature dependence of the potential energy for the crystalline nanoparticle at a temperature of 710 K is associated with the nanoparticle melting, which begins from the nanoparticle surface. The weak peaks in the dependence $U(T)$ at temperatures of 710 and 1200 K for the silicon nanoparticle with the random atomic packing correspond to orientational ordering in the structure. Structural transformations in a nanoassembled particle occur in a smoother manner. There are only weak peaks in the dependence $U(T)$ at temperatures of 410 and 1200 K. The computer simulation of the crystalline and liquid phases of silicon with the use of the isobaric Monte Carlo method and the environment-dependent interatomic potential [16] revealed that, at zero pressure, the weak first-order liquid–liquid phase transition occurs at a temperature of 1135 K and a continuous liquid–amorphous phase transition is observed at 843 K.

According to the Ehrenfest classification [17], phase transitions accompanied by abrupt changes in the first and second derivatives of the thermodynamic potential belong to first-order and second-order transitions, respectively. The melting of bulk crystals is a first-order transition, because this process is attended by an abrupt change in the volume and the entropy. The changeover from massive materials to nanoparticles is accompanied by the enhancement of the surface effect. It is known that the melting temperature T_m of the surface of a massive crystal is lower than the melting temperature T_m of its bulk region and that the melting temperature T_m of nanoparticles decreases with a decrease in their size. For small-sized nanoparticles, jumps in the volume and the entropy are so insignificant that the melting phase transition in these objects can be attributed to second-order phase transitions [18]. For normally melting materials, an increase in the nanoparticle volume can be compensated by the nanoparticle compression under the Laplace pressure. Since the Laplace pressure is inversely proportional to the nanoparticle size, the compensation effect is not observed for large particles and the melting in them occurs as a first-order phase transition. Another situation holds true for anomalous compounds, such as silicon. The melting of the silicon crystal leads to a decrease in the volume; i.e., a skeleton packing transforms into a closer packing. A decrease in the volume due to the melting should have also been observed for silicon nanoparticles. However, since the Si–Si interaction has a short-range nature, more free atoms of the surface move away from the bulk region. As a result, a negative radial gradient of the density arises and a change in the volume upon melting is minimized. Therefore, the Laplace pressure in this case is immaterial due to the specific features of the Si–Si interatomic interaction.

For a crystalline nanoparticle, the temperature dependence of the specific heat at a constant pressure C_p exhibits a sharp peak at a temperature of 710 K. The temperature dependence of the specific heat at a constant pressure for a nanoparticle with a random atomic packing exhibits less pronounced peaks at the aforementioned temperatures. The specific features observed in the dependence $C_p(T)$ for a nanoassembled particle can be mistaken for fluctuations. It is at this temperature of 710 K that the temperature dependence of the self-diffusion coefficient for a crystalline nanoparticle deviates from the linear behavior to the greatest extent (toward a decrease in the self-diffusion coefficient D). The reason for this deviation is that the atomic thermal motion is “blocked” immediately before the onset of the irreversible breaking of the crystal structure [19].

In essence, the phenomenon is as follows. The atomic arrangement in a crystal lattice can be represented as a packing of atomic layers alternating in a

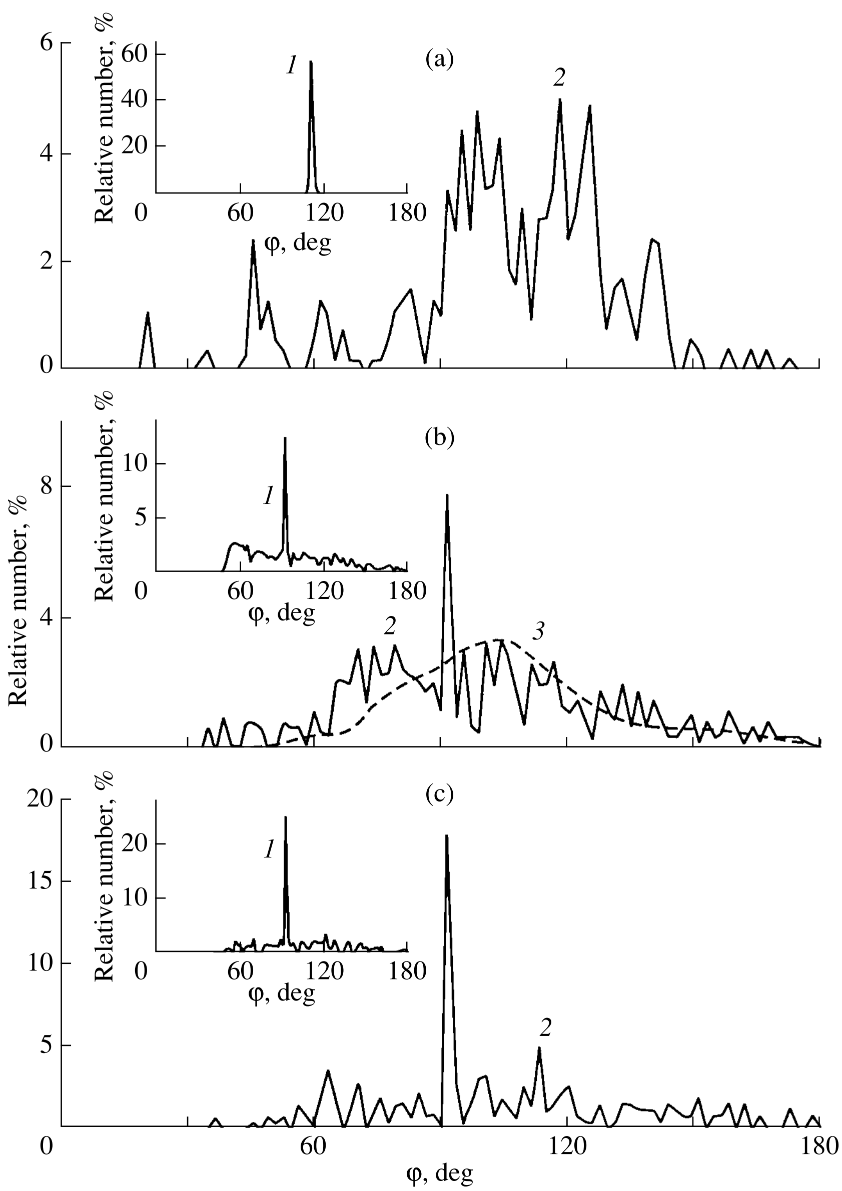

Fig. 5. Distributions of the angles φ between Si–Si bonds in silicon nanoparticles with (a) a diamond-like lattice, (b) a random atomic packing, and (c) a fullerene and an inserted icosahedron according to the molecular dynamics calculations at temperatures of (*1*) 10 and (*2*) 1710 K. (*3*) Distribution of the angles φ in the inner region of the 480-atom silicon nanoparticle at a temperature of 1560 K [14].

specific manner. In the lattice, silicon atoms are held by strong but short-range forces of the covalent interaction. Initially, the lattice does not contain point defects (vacancies, interstitial atoms). At high temperatures, the crystal lattice is distorted, atomic layers are strongly bent, and their identification is complicated. In the vicinity of the melting temperature, the amplitudes of atomic vibrations increase so that individual atoms can break the bonds with atoms of their “layer.” However, they cannot freely pass into the neighboring layer. The transformation of a regular atomic arrangement into an irregular arrangement is a collective process in which motions of individual atoms are hindered. The kinetic limitations in the structural transformation manifest themselves in a drastic decrease in the self-diffusion coefficient. There occurs a “blocking” effect. With a further increase in the temperature of the system, atomic collisions become more frequent and stronger. The number of broken bonds increases sharply. Atoms execute the translational motion, which manifests itself in a considerable increase in the self-diffusion coefficient. The system completely transforms into the liquid state.

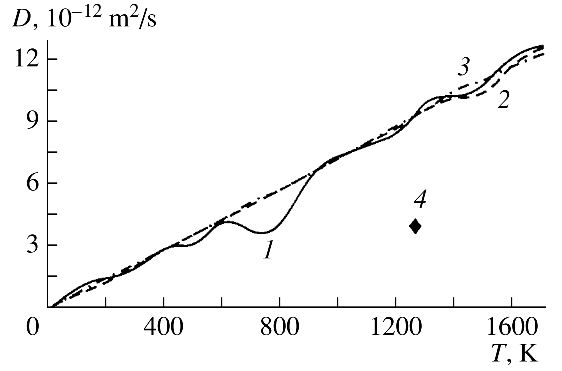

Fig. 6. Temperature dependences of the self-diffusion coefficient of atoms in silicon nanoparticles: (*1*) particle with a diamond-like structure, (*2*) particle with a random atomic packing, and (*3*) nanoassembly composed of a 60-atom fullerene and a 13-atom icosahedron. (*4*) Experimental temperature dependence of the self-diffusion coefficient according to the data taken from [15].

CONCLUSIONS

Over a few last decades, the molecular dynamics method has been widely used for investigating the properties of quite different materials. These are molecular crystals, amorphous polymers, liquid crystals, zeolites, nucleic acids, proteins, superconductors, and semiconductors. In the present work, the structure and thermodynamic properties of 73-atom silicon nanoparticles that had substantially different initial structures were studied over a wide range of temperatures. It was demonstrated that a 73-atom crystalline nanoparticle undergoes melting at temperatures close to 710 K. The melting of a 480-atom silicon nanoparticle is observed at a temperature of 1560 K [14], which is close to the melting temperature of real silicon crystals (1665 K). It was revealed that, as the temperature increases, structural transformations in a nanoassembled silicon particle occur in a smoother manner as compared to those in a silicon nanoparticle with a random atomic packing. The simulation of a silicon nanoparticle constructed from a fullerene and an icosahedron showed that the Tersoff potential with the parameters taken from [7] is not a universal potential. The molecular dynamics calculations based on the density functional theory and the ab initio theory of electronic structure revealed that liquid silicon nanoparticles containing from 274 to 323 atoms can form distorted icosahedral structures upon freezing [20]. A geometrical prerequisite for the explanation of this fact is the possibility of constructing an icosahedron from 20 slightly distorted tetrahedra shared by faces. Thus, the conclusion can be drawn that the computer simulation makes it possible to predict the structure and thermodynamic properties of new noncrystalline materials and to improve the technology used for their production.

ACKNOWLEDGMENTS

This study was supported by the Presidium of the Ural Division of the Russian Academy of Sciences within the framework of the Integration Project of the Ural Division–Far East Division of the Russian Academy of Sciences.

REFERENCES

1. Zhao, Y., Kim, Y.-H., Du, M.-H., and Zhang, S.B., First-Principles Prediction of Icosahedral Quantum Dots for Tetravalent Semiconductors, *Phys. Rev. Lett.*, 2004, vol. 93, p. 015502.
2. Chen, Z., Jiao, H., Seifert, G., Horn, A.H.C., Yu, D., Clark, T., Thiel, W., and von Ragué Schleyer, P., The Structure and Stability of Si_{60} and Ge_{60} Cages: A Computational Study, *J. Comput. Chem.*, 2003, vol. 24, pp. 948–953.
3. Nishio, K., Koga, J., Yamaguchi, T., and Yonezawa, F., Theoretical Study of Light-Emission Properties of Amorphous Silicon Quantum Dots, *Phys. Rev. B: Condens. Matter*, 2003, vol. 67, p. 195304.
4. Park, N.-M., Choi, C.-J., Seong, T.-Y., and Park, S.-J., Quantum Confinement in Amorphous Silicon Quantum Dots Embedded in Silicon Nitride, *Phys. Rev. Lett.*, 2001, vol. 86, pp. 1355–1357.
5. Kim, B.-H., Cho, C.-H., Kim, T.-W., Park, N.-M., Sung, G.-Y., and Park, S.-J., Photoluminescence of Silicon Quantum Dots in Silicon Nitride Grown by NH_3 and SiH_4, *Appl. Phys. Lett.*, 2005, vol. 86, p. 091908.
6. Tersoff, J., New Empirical Model for the Structural Properties of Silicon, *Phys. Rev. Lett.*, 1986, vol. 56, no. 6, pp. 632–635.
7. Tersoff, J., New Empirical Approach for the Structure and Energy of Covalent Systems, *Phys. Rev. B: Condens. Matter*, 1988, vol. 37, no. 10, pp. 6991–7000.
8. Vink, R.L.C., Barkema, G.T., van der Weg, W.F., and Mousseau, N., Fitting the Stillinger–Weber Potential to Amorphous Silicon, *J. Non-Cryst. Solids*, 2001, vol. 282, pp. 248–255.
9. Zhang, L. and Jiang, S., Molecular Simulation Study of Nanoscale Friction for Alkyl Monolayers on Si(111), *J. Chem. Phys.*, 2002, vol. 117, no. 4, pp. 1804–1811.
10. Polukhin, V.A. and Vatolin, N.A., Carbon: From a Melt to a Fullerene, *Rasplavy*, 1998, no. 4, pp. 3–32.
11. *Spravochnik khimika* (A Handbook for Chemists), Nikol'skii, V.P., Ed., Leningrad: Khimiya, 1971, vol. 1 [in Russian].
12. Bellisent, R., Menelle, A., Howells, W.S., Wright, A.C., Brunier, T.M., Sinclair, R.N., and Jansen, F., The Structure of Amorphous Si : H Using Steady-State and Pulsed Neutron Sources, *Physica B* (Amsterdam), 1989, vols. 156–157, pp. 217–219.
13. Kubicki, J.D. and Lasaga, A.C., Molecular Dynamics Simulations of SiO_2 Melt and Glass: Ionic and Covalent Moldels, *Am. Mineral.*, 1988, vol. 73, pp. 941–955.

14. Zachariah, M.R., Carrier, M.J., and Blaisten-Barojas, E., Properties of Silicon Nanoparticles: A Molecular Dynamics Study, *J. Phys. Chem.*, 1996, vol. 100, pp. 14856–14864.
15. Hawa, T. and Zachariah, M.R., Internal Pressure and Surface Tension of Bare and Hydrogen Coated Silicon Nanoparticles, *J. Chem. Phys.,* 2004, vol. 121, no. 18, pp. 9043–9049.
16. Miranda, C.R. and Antonelli, A., Transitions between Disordered Phases in Supercooled Liquid Silicon, *J. Chem. Phys.*, 2004, vol. 120, no. 24, pp. 11672–11676.
17. Bazarov, I.P., *Termodinamika* (Thermodynamics), Moscow: Vysshaya Shkola, 1976 [in Russian].
18. Kawazoe, Y., Kondow, T., and Ohno, K. *Clusters and Nanomaterials: Theory and Experiment*, Berlin: Springer-Verlag, 2002.
19. Baidakov, V.G., Galashev, A.E., and Skripov, V.P., Stability of a Superheated Crystal in the Molecular Dynamics Model of Argon, *Fiz. Tverd. Tela* (Leningrad), 1980, vol. 22, no. 9, pp. 2681–2687 [*Sov. Phys. Solid State* (Engl. transl.), 1980, vol. 22, no. 9, pp. 1565–1568].
20. Nishio, K., Morishita, T., Shinoda, W., and Mikami, M., Molecular Dynamics Simulation of Icosahedral Si Quantum Dot Formation from Liquid Droplets, *Phys. Rev. B: Condens. Matter,* 2005, vol. 72, p. 24532.